SYNTHESIS AND PROPERTIES OF INORGANIC COMPOUNDS

PREPARATION OF HIGH-ENTROPY LAYERED DOUBLE HYDROXIDES WITH A HYDROTALCITE STRUCTURE

O. E. Lebedeva[a], S. N. Golovin[a], E. S. Seliverstov[a], E. A. Tarasenko[a], O. V. Kokoshkina[a], D. E. Smalchenko[a], M. N. Yapryntsev[a]

[a]*Belgorod State National Research University,Belgorod, 308015 Russia*

**e-mail: olebedeva@bsu.edu.ru*

Received July 29, 2024

Revised October 01, 2024

Accepted October 02, 2024

High-entropy hexacationic layered double hydroxides of the cationic composition MgNiCoAlFeY were obtained by five different methods: coprecipitation at constant pH, coprecipitation at constant or variable pH followed by hydrothermal treatment, microwave assisted solvothermal, hydrothermal, mechanochemical method followed by hydrothermal treatment. All samples, except for the one obtained by coprecipitation at variable pH, are phase pure, with a uniform distribution of cations. The samples were characterized by X-ray diffraction, infrared spectroscopy, Raman spectroscopy, transmission electron microscopy. Thermal transformations of the samples were studied. The synthesis method affects the characteristics of the samples. The sample obtained by hydrothermal synthesis at variable pH possesses magnetic properties. The largest particles and those morphologically close to the hexagonal shape are formed by coprecipitation followed by hydrothermal treatment. The sample obtained by the microwave assisted solvothermal method is characterized by lower thermal stability.

Keywords: coprecipitation, hydrothermal treatment, microwave-assisted synthesis, mechanochemical synthesis

DOI: 10.31857/S0044457X250104e1

INTRODUCTION

At the beginning of the 21st century, the concept of high-entropy materials emerged and is actively developing. The main idea underlying it is to maximize the configurational entropy of the material, leading to the minimization of its Gibbs free energy, which allows stabilizing the system and giving the material combined properties that were not previously exhibited by each component separately. High-entropy compounds include those whose configurational entropy exceeds 1.5R(R–

universal gas constant) [1]. Initially, the concept related to metal alloys and intermetallics [2]. Then it began to be applied to compounds of other classes: oxides, nitrides, silicides, etc. [3, 4]. By now, the concept has been extended to compounds of fairly complex composition, among which layered double hydroxides are of considerable interest.

Layered double hydroxides (**LDH**) are a class of natural and synthetic inorganic compounds, the structure of which represents a system of positively charged metal hydroxide brucite-like octahedral layers, alternating with "interlayers" of anions and water molecules. The stability of the structure is due to the electrostatic interaction between the hydroxide layers and interlayer anions [5, 6]. The general formula of layered double hydroxides has the form $M^{2+}_{1-x}M^{3+}_{x}(OH)_2]^{x+}[A^{n-}_{x/n} \cdot y\ H_2O]^{x-}$. The compounds contain di- and trivalent cations and any anions A^{n-}. The first described layered double hydroxide was the mineral hydrotalcite $[Mg_6Al_2(OH)_{16}](CO_3) \cdot 4H_2O$, which gave the name to the entire group of compounds. To date, a large number of different variations of such layered structures have been synthesized, differing in the nature of cations, their molar ratio, as well as the nature of anions. About 20 different cations have been successfully included in the hydrotalcite-like structure, and researchers are not limited to only binary compounds; quite a few three- and four-cation LDHs have been obtained. The range of values $0.2 \leq x \leq 0.33$ is recognized as optimal for synthesis, i.e., the ratio M^{2+}/M^{3+} should lie in the range from 2:1 to 4:1 [5].

The main directions of potential application of LDHs are heterogeneous catalysis [7], anion exchange and adsorption [8], targeted drug delivery [9], manufacturing of phosphors [10] and electrodes for supercapacitors [11].

The compositional flexibility of hydrotalcite-like LDHs makes them promising compounds for obtaining high-entropy layered double hydroxides (**HE LDHs**). The first publication on this topic appeared in 2020 [12]. A five-cation LDH containing

magnesium, aluminum, cobalt, nickel, and zinc cations (MgAlCoNiZn – hereinafter a conventional designation of the LDH cationic composition) was obtained by the coprecipitation method. Most subsequent publications on HE LDHs are devoted to the electrocatalytic properties of these compounds; they proved particularly effective in the process of oxygen evolution from water [13-21]. HE LDHs are also considered as precursors for obtaining high-entropy oxides [22] and electrode materials for supercapacitors [23].

The minimum number of cationic components providing a high value of configurational entropy is five, with the content of all components being comparable. For example, five-cation HE LDHs FeAlCoNiZn, FeCrCoNiZn, and FeCrCoNiCu with near-equimolar cationic component content were obtained by hydrothermal treatment [13]. It is reported that among five-cation layered double hydroxides, samples of NiFeCoZnCr [14], FeCoNiCuZn [15, 16], FeNiCoMnCr [20], NiCoMoMnZn [20], and MnFeCoNiCu decorated with gold atoms [21] have also been obtained. A large series of five-cation LDHs of various compositions is presented in [19]. It should be noted that in most of these works, the obtained samples are insufficiently crystallized or contain impurity phases.

Layered double hydroxides are more likely to crystallize into a high-entropy composition when they contain six or more cationic components. Six- and seven-cation LDHs are presented, for example, in [20]. The content of cationic components in them is close to equimolar. In [24], seven- and eight-cation HE LDHs with the composition MgCuZnCoNiAlFeCr were obtained. Perhaps the most multi-cationic LDH at the moment includes cations of ten metals (MgCoAlNiFeCrCuZnMnGa), uniformly distributed in a single-phase structure [22].

There is a fairly large set of methods for synthesizing LDHs, the most common of which are coprecipitation methods and hydrothermal synthesis; less common are specific methods, such as plasma chemical synthesis [25]. Most HE LDHs have been

obtained using hydrothermal synthesis.

The purpose of this work is to compare several methods for the synthesis of HE LDH using the example of a six-cation layered double hydroxide containing Mg^{2+}, Ni^{2+}, Co^{2+}, Al^{3+}, Fe^{3+} and Y^{3+} cations, as well as to expand the possible set of cations included in HE LDH. We are not aware of any publications on the synthesis of HE LDH containing yttrium cations.

EXPERIMENTAL PART

The following initial reagents were used: magnesium nitrate hexahydrate $Mg(NO_3)_2 \cdot 6H_2O$, nickel(II) nitrate hexahydrate $Ni(NO_3)_2 \cdot 6H_2O$, cobalt(II) nitrate hexahydrate $Co(NO_3)_2 \cdot 6H_2O$, aluminum nitrate nonahydrate $Al(NO_3)_3 \cdot 9H_2O$, iron(III) nitrate nonahydrate $Fe(NO_3)_3 \cdot 9H_2O$, yttrium(III) nitrate hexahydrate $Y(NO_3)_3 \cdot 6H_2O$.

The synthesis of LDH samples was carried out using five different methods. All samples had the same calculated cationic composition (Table 1) established during synthesis.

Synthesis by co-precipitation at constant pH. Samples of all six salts were dissolved in distilled water. The resulting solution and a 1 M solution of NaOH precipitant were simultaneously added dropwise to 150 ml of distilled water with constant stirring. The pH value was maintained at 8-9. The resulting suspension was kept under the mother liquor with constant stirring for 24 hours, and then thermostated at 98°C for 48 hours. The precipitate was decanted, washed with distilled water, and dried at 100°C (sample **LDH-C**).

Co-precipitation at constant pH followed by hydrothermal treatment was carried out using the same method, except for the thermostating stage, instead of which the reaction mixture was placed in a steel reactor and kept at 150°C for 48 hours (sample **LDH-CH**).

Synthesis by co-precipitation at variable pH with hydrothermal treatment

(sample **SDG-G**). The weighed salts were dissolved in distilled water, then a solution of the precipitating agent - sodium hydroxide - was added to the reaction mixture with constant stirring. The resulting mixture was transferred to a reactor chamber, which was then sealed and left at 120°C for 48 h. Then the precipitate was separated from the mother liquor by centrifugation, washed with distilled water until neutral pH and air-dried.

Co-precipitation with solvothermal-microwave treatment (sample **SDG-SM**) was carried out in a Teflon reactor in a closed-type MARS 6 system at 600 W power and a temperature of 120°C for 1 h. Otherwise, the synthesis methodology was similar to co-precipitation with hydrothermal treatment.

Mechanochemical synthesis with subsequent hydrothermal treatment and additional recrystallization (sample **SDG-M**). The weighed salts were ground in an agate mortar. After obtaining a homogeneous powder, dry sodium carbonate Na_2CO_3 and sodium hydroxide NaOH were added, then ground until a viscous homogeneous paste was obtained. The paste was washed into a hydrothermal synthesis vessel. The vessel was sealed and left for a day at a temperature of 98°C. After 1 day, 0.1 M Na_2CO_3 solution was added to the reaction mixture and left for 2 days at a temperature of 98°C. The mixture was cooled, the resulting material was separated from the mother liquor by centrifugation, then washed with distilled water until neutral and dried at 50°C in a thermostat.

X-ray phase analysis was performed using a Rigaku SmartLab X-ray diffractometer (Cu K_α-radiation). The scanning range was $2\theta = 5°–80°$, with a step of 0.02°, at a rate of 2 degrees/min. The average crystallite diameter of SDG was calculated using the Scherrer equation in the (003) and (110) directions. Temperature X-ray phase analysis was carried out using the same equipment, with a recording rate of 5 degrees/min. Initial scanning was performed at 35°C, and then in the range of

100–1000°C with a step of 100°C. The heating rate was 25 degrees/min, with a holding time of 10 min at each temperature.

All synthesized samples were analyzed by FTIR spectroscopy. IR transmission spectra of the synthesized LDHs were obtained on an FSM 2201 FTIR spectrometer (Infraspec LLC, Russia). Samples were prepared by pressing a mixture of potassium bromide with the synthesized sample in a ratio of 100 : 1 respectively.

Raman spectra were recorded on a LabRam HR Evolution Raman confocal microspectrometer (HORIBA Jobin Yvon S.A.S., Japan) using a Nd:YAG laser with a wavelength of 532 nm in the range from 200 to 2000 cm^{-1}.

Examination of samples by X-ray microanalysis (EDS-SEM) and elemental mapping were carried out on an Oxford Instruments X-max 80 energy-dispersive X-ray spectrometer at an accelerating voltage of 30 kV and a working distance of 15 mm.

The morphology of LDH particles was studied by transmission electron microscopy using a JEM-2100 transmission electron microscope (JEOL, Japan) at an accelerating voltage of 200 kV.

RESULTS AND DISCUSSION

The ratio of cations in the composition of LDH samples was chosen for the following reasons. Since the ability of each specific composition to crystallize into a hydrotalcite-like phase is not known in advance, nickel and aluminum cations were introduced into the composition in increased amounts compared to other elements. These cations usually easily form the LDH structure; it was assumed that they would serve as a hydrotalcite matrix for cations of other elements.

According to energy-dispersive analysis, all six cations introduced during synthesis are detected in all obtained samples. However, the content of elements in samples synthesized by different methods differs noticeably. There are also

differences between the actual composition and the planned calculated one. The most significant deviation from the amount laid down during synthesis is aluminum, which exceeds the calculated value in all samples (Table 1), which may be due to the low pH value of complete precipitation of aluminum hydroxide. The LDH-SG sample has the composition closest to the specified one, and it also achieves the highest ratio of M^{2+}/M^{3+}. It is essential that in all synthesized samples, all cations are evenly distributed, as evidenced by the results of elemental mapping performed for all samples (Fig. 1, using the LDH-SG sample as an example).

Identification of the phase composition of the obtained samples based on X-ray diffractograms (Fig. 2) allows us to conclude that structures belonging to the class of hydrotalcite-like compounds were formed in all five samples synthesized by different methods. This is evidenced by the presence of the main hydrotalcite reflections, corresponding to the basal reflections (003), (006), as well as reflections (012), (015), (018), (110), and (113). There are no reflections of foreign phases on the diffractograms. The crystallographic parameters of the obtained compounds are typical for hydrotalcite-like structures (Table 1).

The intensity of lines on the diffractograms differs for samples obtained by different methods. Such differences can be explained by different degrees of crystallinity, as well as structural disorder of the samples and the possible presence of several polytypes. The formation of a polytype depends on a combination of factors, including the composition of the layers, the nature of the interlayer anions, and the water content, which leads to a wide variety of polytypes [26].

IR spectra of LDH samples (Fig. 3) are similar to each other and contain typical bands inherent to hydrotalcite-like compounds. All presented IR spectra show a broad absorption band in the region of 3300–3600 cm^{-1}, corresponding to the vibrations of hydroxides in the metal-hydroxide layers. The shoulder in the range of 2900–2950 cm^{-1} corresponds to stretching vibrations of hydroxyl groups of water

molecules. Absorption bands in the region of 1600–1650 cm^{-1} reflect bending vibrations of water molecules in the interlayer space. All presented samples have absorption bands at 1340–1355 cm^{-1}, which are consistent with stretching vibrations of interlayer nitrate ions. The presence of absorption bands in the spectrum region <1000 cm^{-1} corresponds to metal-oxygen vibrations in the crystal lattice of the synthesized samples.

Figure 4 shows the Raman spectra of the obtained LDHs. In the region of 550 cm^{-1}, a band characteristic of the octahedral structure of brucite-like layers is observed, usually interpreted as stretching vibrations of Me^{2+}-O-Me^{3+} bonds and considered as one of the distinctive features of LDH [27]. The band around 710 cm^{-1} corresponds to nitrate anions. The band in the region of 1050 cm^{-1} is characteristic of all other intercalated anions and, apparently, is represented by carbonate anions, as is the weak band at 1350 cm^{-1}.

The Raman spectrum of the LDH-H sample, containing additional bands, draws attention. This sample also demonstrated another difference from all other samples: it turned out to be the only one exhibiting magnetic properties. For multi-cation samples including ferromagnetic metal cations, this usually means the formation of X-ray amorphous ferromagnetic spinels in the LDH sample composition. For example, we have shown that a similar phenomenon occurs in tetracationic LDHs of MgCoFeAl composition [28]. Apparently, spinel (or spinels) is also formed in the LDH-H sample, which is consistent with the features of its Raman spectrum; for example, a spectrum of magnesium-cobalt spinel has been published, which contains bands with comparable positions: 193, 473, 512, 609 and 676 cm^{-1} [29].

The study of the particle morphology of the synthesized hydrotalcite-like compounds showed that all samples consist of hexagonal or near-hexagonal shaped particles (Fig. 5). In general, the particle shape of the obtained LDHs is typical for compounds of this class. Interestingly, the largest and well-crystallized hexagonal

particles were obtained by co-precipitation at variable pH followed by hydrothermal treatment in the case of the LDH-H sample, which exhibits magnetic properties.

Investigation of thermal transformations of LDH-H, LDH-CM and LDH-M samples showed that when heated, they behave in a very typical manner for LDHs, decomposing to form mixed oxides of non-stoichiometric composition (Fig. 6). The samples show differences in thermal stability: on the diffractograms of two samples, the reflections characteristic of LDHs disappear at temperatures >300°C, while in the case of LDH-CM they are not observed above 200°C. With further temperature increase >800°C, the appearance of spinel phases is observed.

To conclude whether the obtained LDH samples can be classified as high-entropy compounds, it is necessary to calculate their configurational entropy. It should be noted that the method of calculating this parameter for compounds with complex composition is debatable. For alloys and intermetallics, the validity of applying the solid solution model and the formula is generally recognized:

$$\Delta S_{conf} = -R \sum_{i=1}^{N} x_i \, ln x_i \,, \qquad (1)$$

where x_i – molar fractions of the constituent elements.

However, for oxides, corrections are already made to this formula, requiring separate accounting of possible configurations of ions in cationic and anionic positions [30]. In work [31], an approach is proposed according to which, when calculating the configurational entropy of complex compounds, it is necessary to consider the number of possible configurations of structural elements in all sublattices of the compound.

Calculation of the configurational entropy of LDHs synthesized in this work using formula (1) leads to values in the range of (1.38–1.43) R , J/(mol K). However, when taking into account the anionic composition of the samples, the calculated entropy value increases. Spectroscopic data presented above indicate the presence of three types of anions in the LDH composition: hydroxides, carbonates, and nitrates.

Even with the predominance of one of these anion types, the small contribution of the others and the microstates they form are sufficient for the configurational entropy to exceed the threshold value of 1.5 R . This allows us to state that our LDH samples belong to the category of high-entropy materials.

CONCLUSION

The conducted studies have shown that six-cation high-entropy layered double hydroxides with a hydrotalcite structure can be obtained by various methods. The production method affects the phase purity of the samples and such characteristics as particle size and shape, and thermal stability. The introduction of yttrium cations into the LDH composition does not cause complications with crystallization or the formation of foreign phases.

In the future, virtually all tested methods of HE LDH synthesis can be applied to obtain not only six-cation compounds but also those containing 7–10 different cations in the structure of the brucite-like layer. Increasing the number of components will significantly increase the configurational entropy of the resulting compounds.

ACKNOWLEDGMENT

The authors thank the Center for Collective Use "Technologies and Materials of Belgorod State University" for the opportunity to use the equipment base and consultations of specialists, as well as the Department of Structural Research of the IOC RAS for assistance in performing X-ray microanalysis and elemental mapping.

FUNDING

The study was supported by the Russian Science Foundation (grant No. 24-23-00182).

COMPLIANCE WITH ETHICAL STANDARDS

This work does not contain studies conducted on humans or animals.

CONFLICT OF INTEREST

The authors of this work declare no conflict of interest.

REFERENCES

1. *Yeh J.-W.* // JOM. 2013. V. 65. № 12. P. 1759. https://doi.org/10.1007/s11837-013-0761-6
2. *Yeh J.-W., Chen S.-K., Lin S.-J. et al.* // Adv. Eng. Mater. 2004. V. 6. № 5. P. 299. https://doi.org/10.1002/adem.200300567
3. *Musico B.L., Gilbert D., Ward T.Z. et al.* // APL Mater. 2020. V. 8. № 4. P. 040912. https://doi.org/10.1063/5.0003149
4. *Teplonogova M.A., Yapryntsev A.D., Baranchikov A.E., Ivanov V.K.* // Inorg. Chem. 2022. V. 61. № 49. P. 19817. https://doi.org/10.1021/acs.inorgchem.2c02950
5. *Cavani F., Trifiro F., Vaccari A.* // Catal. Today. 1991. V. 11. № 2. P. 173. https://doi.org/10.1016/0920-5861(91)80068-K
6. *Tretyakov Yu.D., Lukashin A.V., Eliseev A.A.* //Russ. Chem. Rev. 2004. V. 73. N 9. P. 899. https://doi.org/10.1070/RC2004v073n09ABEH000918
7. *Mohapatra L., Parida K.* // J. Mater. Chem. A. 2016. V. 4. № 28. P. 10744. https://doi.org/10.1039/C6TA01668E
8. *Zumreoglu-Karan B., Ay A.N.* // Chem. Pap. 2012. V. 66. № 1. P. 1. https://doi.org/10.2478/s11696-011-0100-8
9. *Mishra G., Dash B., Pandey S.* // Appl. Clay Sci. 2018. V. 153. P. 172. https://doi.org/10.1016/j.clay.2017.12.021

10. *Sonoyama N., Takagi K., Yoshida S. et al.* // Appl. Clay Sci. 2020. V. 186. P. 105440. https://doi.org/10.1016/j.clay.2020.105440
11. *Patel R., Park J.T., Patel M. et al.* // J. Mater. Chem. A. 2018. V. 6. № 1. P. 12. https://doi.org/10.1039/C7TA09370E
12. *Miura A., Ishiyama S., Kubo D. et al.* // J. Ceram. Soc. Jpn. 2020. V. 128. № 7. P. 336. https://doi.org/10.2109/jcersj2.20001
13. *Gu K., Zhu X., Wang D. et al.* // J. Energy Chem. 2021. V. 60. P. 121. https://doi.org/10.1016/j.jechem.2020.12.029
14. *Jing J., Liu W., Li T. et al.* // Catalysts. 2024. V. 14. № 3. P. 171. https://doi.org/10.3390/catal14030171
15. *Junchuan Y., Wang F., He W. et al.* // Chem. Commun. 2023. V. 59. P. 3719. https://doi.org/10.1039/D2CC06966K
16. *Hao M., Chen J., Chen J. et al.* // J. Colloid Interface Sci. 2023. V. 642. P. 41. https://doi.org/10.1016/j.jcis.2023.03.152
17. *Nguyen T.X., Tsai C.-C., Nguyen V.T. et al.* // Chem. Eng. J. 2023. V. 466. P. 143352. https://doi.org/10.1016/j.cej.2023.143352
18. *Wang F., Zou P., Zhang Y. et al.* // Nat. Commun. 2023. V. 14. P. 6019. https://doi.org/10.1038/s41467-023-41706-8
19. *Ding Y., Wang Z., Liang Z. et al.* // Adv. Mater. 2023. P. e2302860. https://doi.org/10.1002/adma.202302860
20. *Li S., Tong L., Peng Z. et al.* // J. Mater. Chem. A. 2023. V. 11. P. 13697. https://doi.org/10.1039/D3TA01454A
21. *Wu H., Zhang J., Lu Q. et al.* // ACS Appl. Mater. Interfaces. 2023. V. 15. № 32. P. 38423. https://doi.org/10.1021/acsami.3c05781
22. *Kim M., Oh I., Choi H. et al.* // Cell Rep. Phys. Sci. 2022. V. 3. № 1. P. 100702. https://doi.org/10.1016/j.xcrp.2021.100702
23. *Zhu Z., Zhang Y., Kong D. et al.* // Small. 2024. V. 20. P. 2307754.

https://doi.org/10.1002/smll.202307754

24. *Knorpp A.J., Zawisza A., Huangfu S. et al.* // RSC Adv. 2022. V. 12. № 40. P. 26362. https://doi.org/10.1039/D2RA05435C

25. *Agafonov A.V., Shibaeva V.D., Kraev A.S., Sirotkin N.A., Titov V.A., Khlyustova A.V.* // *Russ. J. Inorg. Chem.* 2023. V. 68. P.1. https://doi.org/10.1134/S0036023622601842

26. *Leont'eva N.N., Drozdov V.D., Bel'skaya O.B., Cherepanova S.V.* // Russ. J. Gen. Chem. 2020. V. 90. № 3. P. 509. https://doi.org/10.1134/S1070363220030275

27. *Benício L.P.F., Eulálio D., Guimarães L. de M. et al.* // Mater. Res. 2018. V. 21 № 6. P. e20171004. https://doi.org/10.1590/1980-5373-MR-2017-1004

28. *Nestroinia O.V., Ryl'tsova I.G., Yapryntsev M.N., Lebedeva O.E.* // Inorg Mater. 2020. V. 56. P. 747. https://doi.org/10.1134/S0020168520070109

29. *Silambarasan M., Ramesh P.S., Geetha D., Venkatachalam V.* // J. Mater. Sci.: Mater. Electron. 2017. V. 28. P. 6880. https://doi.org/10.1007/s10854-017-6388-6

30. *Rost C.M., Sachet E., Borman T. et al.* // Nat. Commun. 2015. V. 6. P. 1. https://doi.org/10.1038/ncomms9485

31. *Dippo O.F., Vecchio K.S.* // Scripta Mater. 2021. P. 113974. https://doi.org/10.1016/j.scriptamat.2021.113974

Table 1. Cationic composition, unit cell parameters and average crystal diameter of LDH obtained by different methods

Sample	Cationic composition, at.%						M^{2+}/M^{3+}	a, Å	c, Å	d_{003}, nm	d_{110}, nm
	Ni^{2+}	Co^{2+}	Mg^{2+}	Al^{3+}	Fe^{3+}	Y^{3+}					
Calculated composition	45.0	15.0	15.0	20.0	2.5	2.5	3.0				
LDH-S	43.0	14.0	12.0	26.0	2.5	2.5	2.2	3.05	23.63	4.5	4.5
LDH-SH	45.0	15.0	11.0	25.0	2.5	1.5	2.4	3.05	23.83	5.5	8.5
LDH-SM	43.0	15.0	12.0	25.0	2.0	3.0	2.3	3.06	23.21	5.7	15.7
LDH-H	38.0	11.0	19.0	29.0	1.0	2.0	2.1	3.07	23.50	12.6	33.7
LDH-M	39.0	12.0	17.0	28.0	2.0	2.0	2.1	3.05	23.27	11.5	13.8

FIGURE CAPTIONS

Fig. 1. Results of elemental mapping of LDH-SH sample.

Fig. 2. Powder X-ray diffraction patterns of LDH samples: *1* – LDH-S; *2* – LDH-SH; *3* – LDH-H; *4* – LDH-SM; *5* – LDH-M.

Fig. 3. FTIR spectra of LDH: *1* – LDH-SH; *2* – LDH-SM; *3* – LDH-M; *4* – LDH-H; *5* – LDH-S.

Fig. 4. Raman spectra of LDH samples: *1* – LDH-M; *2* – LDH-H; *3* – LDH-SM; *4* – LDH-SH; *5* – LDH-S.

Fig. 5. TEM micrographs: a – LDH-SM, b – LDH-H, c – LDH-SH, d – LDH-M, e – LDH-S.

Fig. 6 . Powder X-ray diffractograms recorded at different temperatures: a - LDH-CM; b - LDH-M; c - LDH-H.

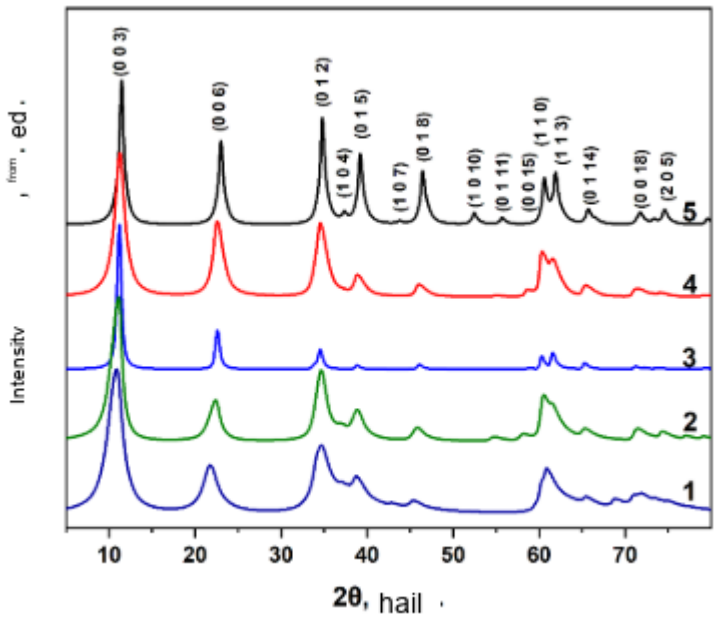
(0 0 3)
(0 0 6)
(0 1 2)
(1 0 4)
(0 1 5)
(1 0 7)
(0 1 8)
(1 0 10)
(0 1 11)
(0 0 15)
(1 1 0)
(1 1 3)
(0 1 14)
(0 0 18)
(2 0 5)
5
4
3
2
1
Intensity
10
20
30
40
50
60
70
2θ, hail

Fig. 1

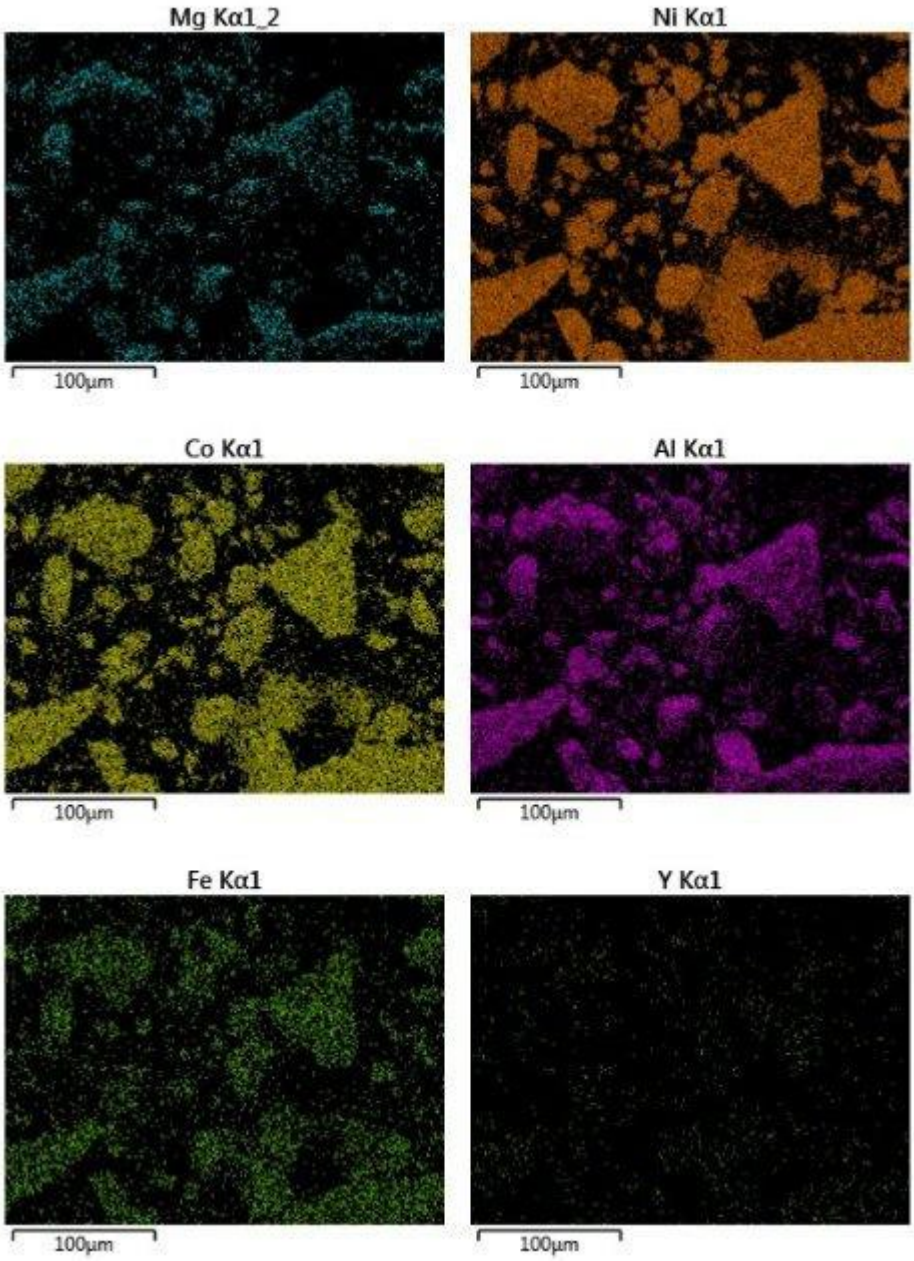
Mg Kα1_2
100μm
Ni Kα1
100μm
Co Kα1
100μm
Al Kα1
100μm
Fe Kα1
100μm
Y Kα1
100μm

Fig. 2

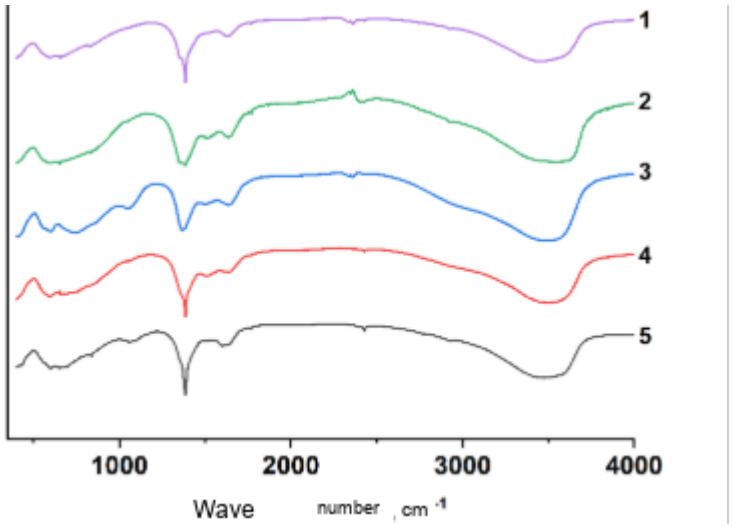
1
2
3
4
5
1000
2000
3000
4000
Wave number , cm -1

Fig. 3

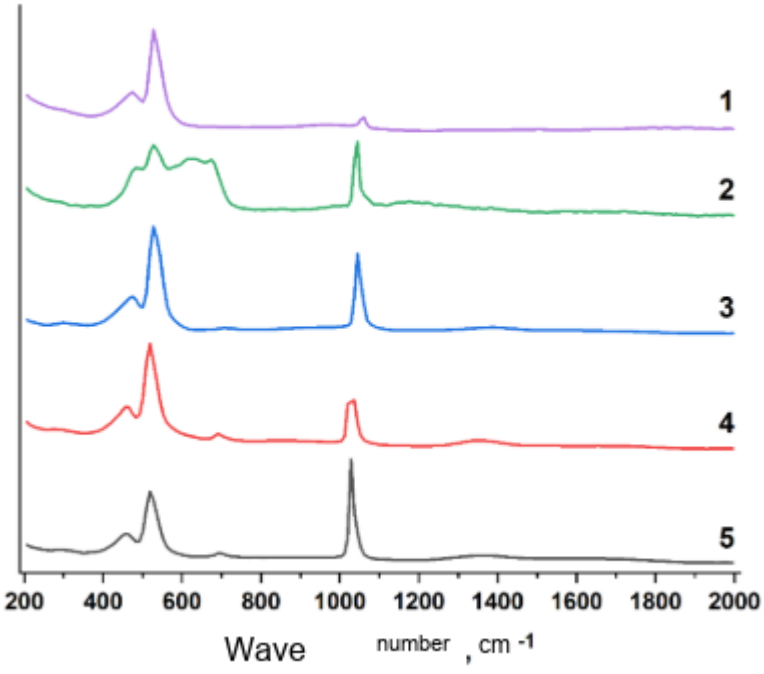
1
2
3
4
5
200
400
600
800
1000
1200
1400
1600
1800
2000
Wave number , cm -1

Fig. 4

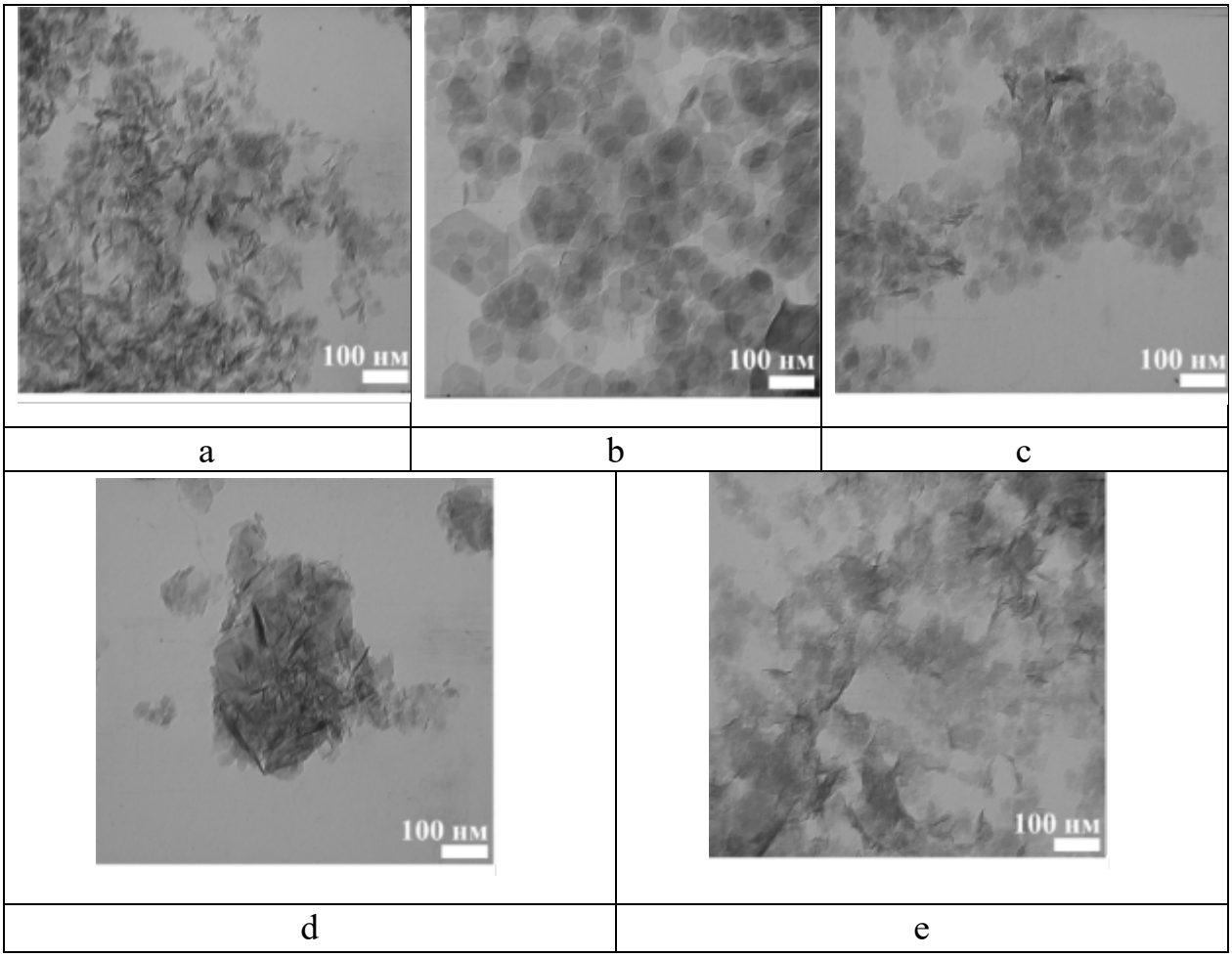

Fig. 5

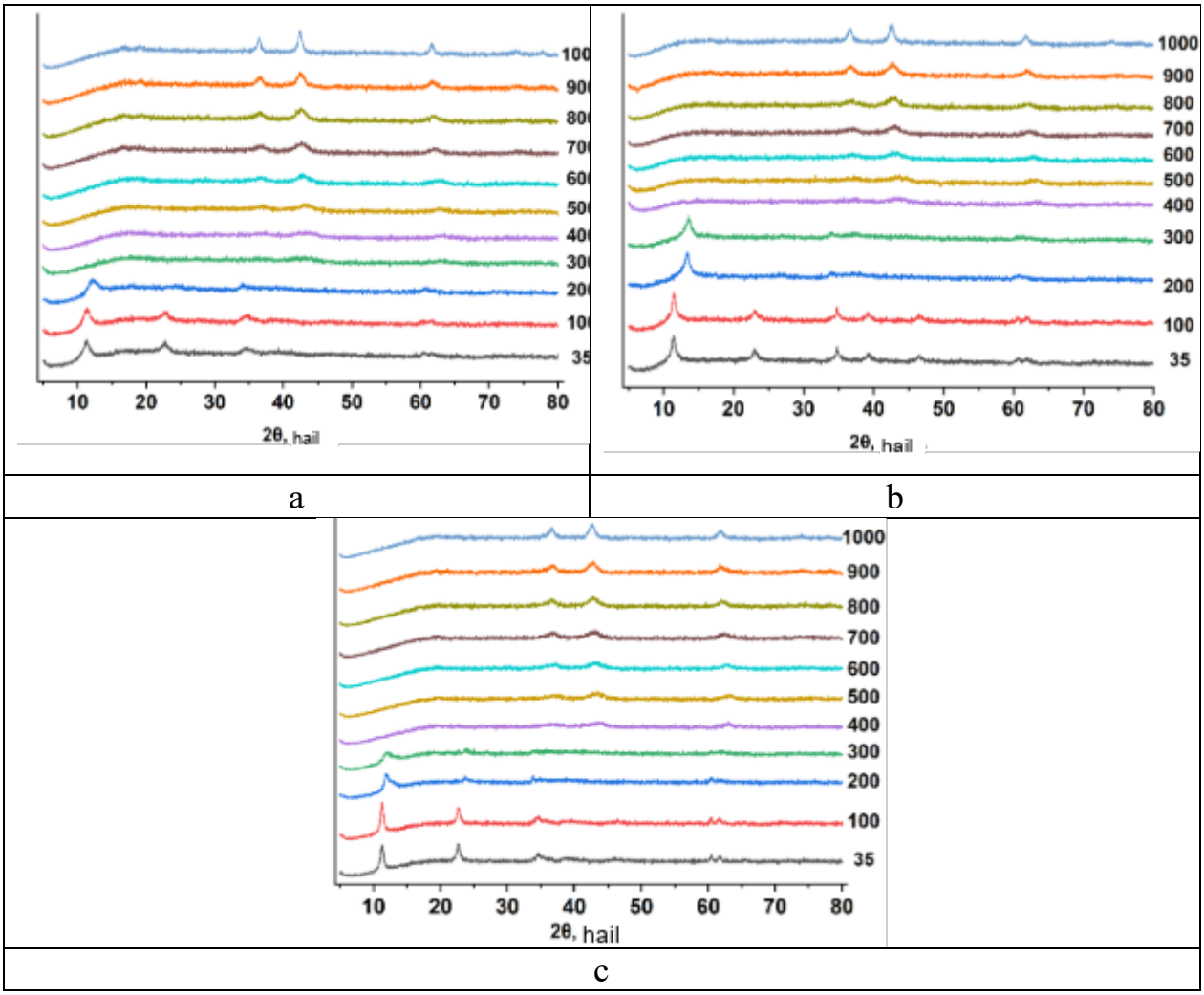
1000
900
800
700
600
500
400
300
200
100
35
10 20 30 40 50 60 70 80
2θ, hail
a
b
c

Fig. 6